Accepted Manuscript

Analytical Methods

PAPER

Geometrically controlled preparation of various cell aggregates by droplet-based microfluidics†

Yaolei Wang,[a] Lei Zhao,[b] Chang Tian,[b] Chao Ma[b] and Jinyi Wang*[ab]

Development of a robust method for the preparation of cell aggregates with different shapes is one of the eager requirements in tissue engineering, since they can be used as building blocks to mimic complex architectures in tissues. Herein, we describe a microfluidic droplet-based approach that can easily produce different shapes of cell aggregates in Ca-alginate microparticles by changing alginate and $CaCl_2$ concentrations. Using this approach, human cervical carcinoma, human hepatocellular liver carcinoma and human umbilical vein endothelial cell aggregates with spherical, spindle- and branch-like shapes were successfully obtained in a repeatable and controllable manner. Cytoskeletal analysis and SEM observation showed that the cell aggregates were densely packed and interconnected. Cell viability assays showed that the viabilities of the retrieved cells from the Ca-alginate microparticles were all more than 95% with good morphology and proliferation ability. Study on the formation mechanism revealed that the shape and size of the cell aggregates were mainly decided by the inner structures of Ca-alginate microparticles, which can be controlled by regulating their preparation conditions. This approach may possess great potential for the construction of various building blocks in tissue engineering with simplicity, controllability, applicability and practicality.

Introduction

In the current medicine, there is an eager demand for native or artificial tissues to repair injured, degenerated or congenitally defected tissues. Transplantation of native tissues is extremely limited by a donor shortage.[1] As a result, the technology of tissue engineering that can provide man-made organs or tissues for transplantation has emerged to meet the requirement.[2] Traditional strategies for tissue engineering always employ a "top-down" approach, in which cells are seeded on a biodegradable polymeric scaffold, and are expected to populate in the scaffold and create their own extracellular matrix.[3] In spite of some thin or avascular tissues, such as bladder, cartilage and skin,[4-6] having been successfully engineered by the "top-down" approach, the fabrication of complex and large tissues (e.g., liver and heart) with high cell densities still faces challenges.[7] This is mainly because dissociated cells in biomimetic scaffolds cannot typically reconstitute the complex structure or function of tissues without pre-organization into the correct 3D geometry.[8] Therefore, the "top-down" methods often meet difficulties in recreating the intricate microstructural features of large tissues. Currently, "bottom-up" approaches are emerging as valuable and alternative means for engineering large tissues by pre-organizing groups of cells into tissue-like structures.[9] Distinct from the "top-down" approaches, in the "bottom-up" methods, objects that are generated by linking simplified building blocks together can be structurally organized at larger length scales.[10] In addition, directing the assembly of building blocks from the "bottom-up" may provide enhanced control over the relative spatial arrangement of cells in engineered tissues.[11] Therefore, fabrication of building blocks is the vital premise in the "bottom-up" approach.[1] Cell spheroid is a common used building block because of its accuracy in simulating *in vivo* tissue microenvironment,[12] which can form through self-assembly by using conventional methods, such as hanging drop,[13-15] gyratory rotation,[16,17] and liquid overlay culture.[18] However, these methods suffered from some disadvantages, such as cell damage due to shear stress, low yield and the difficulty in controlling cell spheroid size.[19,20] To overcome these challenges, micro-manufacturing technologies such as microarrays,[21] microwells,[22] and microfluidic devices[23] have been used to form cell spheroids. More recently, microfluidic droplet-based cell encapsulation in hydrogel microparticles has been also used for spheroid formation, owing to their inherent advantages such as high throughput, versatility and low cost.[24-26]

Classical examples of the use of cell spheroids for building a complex tissue environment are pituitary gland,[27] pancreatic tissue,[28] and cardiac muscle.[29] Although the complex tissues could be engineered by cell spheroids, the building blocks could not be confined to spherical shape because some features are not present in spheroids (e.g., local deformation).[12] Thus, more kinds of shapes of cell aggregates, such as sheets, fibers or other types of cellular aggregates, should be created as

[a.] College of Science, Northwest A&F University, Yangling, Shaanxi 712100, China. Fax: +86-298-708-2520; Tel: +86-298-708-2520; Email: jywang@nwsuaf.edu.cn
[b.] College of Veterinary Medicine, Northwest A&F University, Yangling, Shaanxi 712100, China.

building blocks in the "bottom-up" approach. To date, many approaches have been developed to form non-spheroid cell aggregates, such as micro-fabrication of cell-laden hydrogel,[30,31,33] direct printing of tissues[32] and micromolding.[34-36] For examples, Rivron *et al.* developed a micro-fabrication method to generate different shapes of tissues by co-culturing cell aggregates.[31] Dean *et al.* self-assembled rat hepatoma and human fibroblasts into cell aggregates with the shapes of rods, tori and honeycombs by using micro-molded and non-adhesive agarose hydrogels.[34] Tekin *et al.* developed a patterning method to control spatial arrangement of multiple cell types in defined geometry by utilizing the shape changing property of poly(N-isopropylacrylamide)-based dynamic microstructures.[35] In addition, by using initiated chemical vapor deposition, the same group fabricated PNIPAAm-based microgrooves to develop geometrically controlled and harvestable longitudinal tissue constructs.[36] All the studies greatly revealed the prominent advantages of the micro-engineered methods in the formation of cell aggregates with different shapes. However, some drawbacks such as tedious, labor intensive and limited in the scope of mass production are still needed to be improved. Therefore, simple and popularized methods for the controllable formation of cell aggregates with different shapes remain necessary for the preparation of building blocks in the "bottom-up" approach.

Based on Ca-alginate microparticles,[37] herein, we present a simple, versatile and reproducible approach for the formation of cell aggregates with different shapes. Alginate is a block copolymer that cross-links in the presence of divalent cations such as Ca^{2+}.[38] Because of its biodegradability, rapid solidification by calcium ions, and high permeability to nutrients, alginate is a widely used material for creating cell scaffolds in tissue engineering.[39] In this study, human cervical carinoma (HeLa), human hepatocellular liver carcinoma (HepG2) and human umbilical vein endothelial cell (HUVEC) aggregates with spherical, spindle- and branch-like shapes were obtained in Ca-alginate microparticles produced by using different concentrations of alginate and $CaCl_2$. The formed cell aggregates have uniform size and can be easily retrieved from the alginate microparticles with high viability. In addition, the formation mechanism of the shape-controlled cell aggregates was studied by observing the inner structure of the Ca-alginate microparticles through the epoxy semi-thin sections of them.

Experimental

Materials and reagents

RTV 615 polydimethylsiloxane (PDMS) prepolymer and curing agent were purchased from Momentive Performance Materials (Waterford, NY, USA). The surface-oxidized silicon wafers were obtained from Shanghai Xiangjing Electronic Technology Ltd. (Shanghai, China). The AZ 50XT photoresist and developer were bought from AZ Electronic Materials (Somerville, NJ, USA). SPI-Pon™ 812 Epoxy Embedding Kit, acridine orange (AO), propidium iodide (PI), Hoechst 33258, A0682-100G sodium alginate, sodium citrate, M8410 mineral oil, S6760 sorbitan monooleate (Span 80), Hexamethyl Disilazane (HMDS), glutaraldehyde and osmium were purchased from Sigma-Aldrich (MO, USA). The cell culture medium, fetal bovine serum (FBS), trypsin, and TRITC-phalloidin were obtained from Gibco Invitrogen Corporation (CA, USA). All solvents and other chemicals were purchased from local commercial suppliers and were of analytical reagent grade, unless otherwise stated. All solutions were prepared using ultrapurified water supplied by a Milli-Q system (Millipore).

Device fabrication

The microfluidic device used in this study was fabricated using soft lithography with PDMS.[40] First, we designed patterns for the channels and chambers using the software AutoCAD. Next, the channels and chambers were printed at 2,000 dots per inch on transparent films (MicroCAD Photomask Ltd., Suzhou, China) and used as the photomask. Then, a mold (30 μm high) was fabricated in a single step under UV light using an AZ 50XT Photoresist on a BG-401A mask aligner (7 mW cm^{-2}; CETC, China).

Before fabricating the microfluidic device, the mold was exposed to trimethylchlorosilane vapor for 3 min.[41] A mixture of PDMS [RTV 615 A and B (10 : 1, w/w)] was then poured onto the mould to yield a 3 mm-thick fluidic layer. After degassing, the mould was baked for 30 min at 85 °C. Then, the PDMS layer structure was peeled from the mold. Holes were punched with a metal pin at the terminals of the inlet and outlet channels. Next, the fluidic layer was placed on top of a glass slide (3000 rpm, 45 s, ramp 15 s) coated with a thin PDMS film [RTV 615 A and B (5:1)] that was cured for 20 min in an oven at 80 °C.[42] The microfluidic device was then ready for use after baking at 80 °C for 72 h.

Cell culture

HeLa, HepG2 and HUVECs were obtained from the Chinese Academy of Sciences (Shanghai, China). The cells were cultured using Dulbecco's Modified Eagle Medium (DMEM) supplemented with 10% FBS, 100 U mL^{-1} penicillin and 100 μg mL^{-1} streptomycin in a humidified atmosphere of 5% CO_2 at 37 °C. The cells were normally passaged at a ratio of 1:2 every 3 days to maintain them in the exponential growth phase. When the cells reached confluence, they were harvested through trypsinization with 0.25% trypsin in phosphate buffered saline (PBS, pH 7.4) at 37 °C.[26,44,45] The PBS solution consisted of 8.00 g/L NaCl, 0.20 g/L KCl, 0.20 g/L KH_2PO_4, and 2.90 g/L $Na_2HPO_4 \cdot 12H_2O$, and pH values were adjusted with 1.0 M HCl and 1.0 M NaOH. Trypsinization was stopped by adding freshly supplemented DMEM. The cell suspension was centrifuged at 1000 rpm for 3 min. The cells were then resuspended in supplemented DMEM for further use.

Ca-alginate microparticle formation and cell encapsulation

Sodium alginate solutions (0.5%, 1%, 2% and 3%, w/w) and $CaCl_2$ solutions (2.5%, 5% and 10%, w/w) were prepared by dissolving sodium alginate (0.5 g, 1 g, 2 g and 3 g) and $CaCl_2$ (2.5 g, 5 g and 10 g) in 100 g DMEM, respectively. Before use,

alginate solutions, $CaCl_2$ solutions and mineral oil with 5% (w/w) Span 80 were filtered with a 0.22-μm syringe filter (Millex-GV, Millipore) for sterilization.[26] HeLa, HepG2 and HUVEC suspensions were respectively prepared by suspending cells in the sodium alginate solutions with a density of 1×10^7 cell mL^{-1}. For producing droplets, the dispersed phase was the cell suspension. Mineral oil was used as an immiscible solvent and 2% (w/w) Span 80 was added to the mineral oil to stabilize the droplets.[43] All solutions were introduced into the microfluidic channel using a syringe pump (LSP01-1A, Baoding Longer Precision Pump Co., Ltd., Hebei, China). By connecting a Teflon tube (ID 0.6 mm and OD 0.8 mm) to the outlet, the formed droplets were transported and collected in a $CaCl_2$ bath and gelled. Afterward, the gelled Ca-alginate microparticles were washed with PBS, centrifuged at 500 rpm for 5 min and collected into a 35-mm cell culture dish (Nunc, Denmark). The cell-encapsulated Ca-alginate microparticles were cultured in a humidified atmosphere of 5% CO_2 at 37 °C for 4 days and the medium was changed everyday.

Cell staining

Cell viability assessment was performed using a common AO/PI staining protocol.[44] Following by removing the growth medium and washing with PBS carefully, the AO/PI staining solution (10 μg mL^{-1} each in PBS) was introduced into the culture dish and the staining process was performed for 10 min at room temperature. Then, PBS was introduced for 10 min as a final rinse. For a clear visualization of cytoskeleton, the actin filament of cells was also stained.[45] Briefly, the cell aggregates were fixed using 4% paraformaldehyde for 30 min at room temperature after washing thrice with PBS. Then, the cells were permeabilized with PBS containing 0.2% Triton X-100 for 30 min. Finally, the cell aggregates were incubated at 37 °C for 20 min with TRITC-phalloidin (100 nM in PBS). The cell aggregates were also incubated for 10 min in PBS containing H33258 fluorochrome (0.5 μg mL^{-1}) for nuclear staining.

### Retrieval and reculture of the cell aggregates

After cell aggregate formation, they were retrieved from the Ca-alginate microparticles by dissolving the Ca-alginate microparticles in 55 mM sodium citrate buffered with 10 mM PBS (pH 7.4) for 10 min at room temperature. For reculture of the formed cell aggregates, they were first washed thrice with PBS after being released from the Ca-alginate microparticles and then were cultured in a 6-well culture plate using DMEM supplemented with 10% FBS, 100 U mL^{-1} penicillin and 100 μg mL^{-1} streptomycin in a humidified atmosphere of 5% CO_2 at 37 °C for 72 h. The culture medium was changed everyday.

Scanning electron microscopy

Growth media was removed and 55 mM sodium citrate buffered with 10 mM PBS (pH 7.4) was added for 10 min to dissolve the Ca-alginate microparticles. After washing thrice with PBS, the pre-warmed (37 °C) 2% glutaraldehyde (Sigma-Aldrich, UK) in 0.1 M sodium cacodylate buffer was added and cells were fixed at room temperature for 60 min. The fixative was then removed and cells was washed thrice (over 5 min each) in 0.1 M sodium cacodylate buffer, before adding 2% osmium in distilled water for 30 min. Cells were washed again with buffer before being dehydrated through a graded series of alcohols (30%, 50%, 70%, 90% and 100% ×3; 10 min at each concentration), then gradually transferred through a graded series of HMDS (i.e. 100% ethanol, 30% HMDS, 50% HMDS, 70% HMDS and 100% HMDS; 10 min at each stage). The samples are then left to dry in a vacuum freeze dryer overnight before Cr/Au (~15 nm) was deposited by E-beam evaporation.

Inner structure analysis of the Ca-alginate microparticles

A semi-thin section of epoxy resin method was used for observing the inner structure of Ca-alginate microparticles.[46] Ca-alginate microparticles were first rinsed thrice with PBS and then with 30%, 50%, 70%, 80%, 90% and 100% (v/v) ethanol step by step to dehydrate.[46] After that, Ca-alginate microparticles were immersed in various ethanol and glue mixtures for 3 h (ethanol :
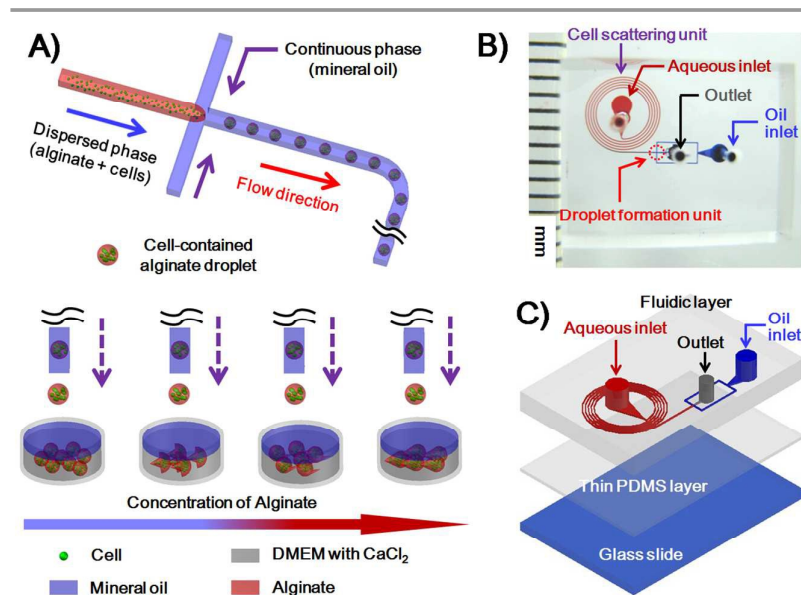
Fig. 1 Schematic illustration of the experimental setup. A) Illustration of microfluidic emulsification coupled with the crosslinking reaction process between alginate and $CaCl_2$. Uniform water droplets containing different concentration of alginate and cells dispersed in mineral oil containing 2% w/w Span 80 were generated in a flow focusing microfludic device. The droplets were collected into a gelation bath in which a double layer of two solutions was contained: the upper mineral oil layer with 2% w/w Span 80, and the bottom aqueous layer with different concentration of $CaCl_2$ in DMEM, acting as a crosslinking agent. B) An overview of the actual microfluidic device. The various channels were loaded with two food dyes to help visualize the different microfluidic components (red dye represents aqueous phase and blue dye represents oil phase). C) Composition of the device: the three layers are sequentially shown from top to bottom, namely, the fluidic layer, thin PDMS layer, and glass slide.

glue = 3:1, v/v), 6 h (ethanol : glue = 1:1, v/v) and 12 h (ethanol : glue = 1:3, v/v) at room temperature, respectively. The glue was prepared with 2-dodecen-1-ylsuccinic anhydride (DDSA), methylnadic anhydride (NMA) and SPI-PON 812 resin (7:14:20, v/v/v) following the manufacturer's instructions. Then, the Ca-alginate microparticles were immersed in pure glue for 48 h at room temperature and 48 h at 55 °C, respectively. Finally, the Ca-alginate microparticles encapsulated in the solidified glue were cut off into 2-μm slices with LEICA Rm 2265 microtome. To visualizing the inner structure of microparticles, the slices were stained with methylene blue for 5 min.[47]

Microscopy and image analysis

An inverted microscope (Olympus, CKX41) with a charge coupled device camera (Olympus, DP72) and a mercury lamp (Olympus, U-RFLT50) was used to obtain phase-contrast and fluorescence images. Confocal Laser Scanning Microscopy (CLSM) images were acquired with an Olympus FV 1000 confocal microscope. A scanning electron microscope (SEM; JSM-6360LV) was used to determine the morphology of the recovered cell aggregates. The image and data analyses were performed using Image-Pro Plus 6.0 (Media Cyternetics, Silver Spring, MD) and SPSS 12.0 (SPSS Inc.), respectively. The results, including the error bars in the graphs, were given as the mean ± standard deviation.

Results and discussion

Design of the system for cell aggregate formation

To continuously generate Ca-alginate microparticles for cell aggregate formation, a system combined with a microfluidic device and a reservoir pool was designed in the present study (Fig. 1A). Generally, the microfluidic device is composed of two PDMS layers (Fig. 1B and C). The fluidic layer includes a cell scattering unit and a droplet formation unit. The cell scattering unit consists of a 5-loop curved microchannel (50 μm width, 30 μm height and 100 μm spatial interval) and one inlet for the introduction of cell and alginate mixture. After passing through the curved microchannel, affecting by the Dean force, cells were separated.[48] The droplet formation unit was composed of an oil channel (100 μm width and 30 μm height), a cross junction and one outlet. The oil and aqueous solutions meet at the cross junction and spontaneously generate a droplet due to their different interfacial properties.[43] The thin PDMS layer on the glass slide was used for irreversibly sealing the channel network in the fluidic layer.[42] Inlets and outlet in the device were used for loading, purging and removing processes. The reservoir pool contained a double layer of two solutions: the upper

mineral oil layer with 2% w/w Span 80, and the bottom DMEM layer with different concentrations of $CaCl_2$. Emulsion droplets would change their shape inside the collecting tubing due to confinement effect of the tubing.[49] The upper layer was used for helping Na-alginate droplets to recover spherical shape before gelation[50] and the bottom layer of $CaCl_2$ solution acting as a crosslink agent.[26] As showed in Fig. 1A, alginate solution with cells and mineral oil contained 2% w/w Span 80 were introduced into the inlet channel to establish the flow system. Uniform Na-alginate droplets generated at the cross-junction of the device and dripped into the reservoir pool through a Teflon tube connected to the outlet. Then, the Na-alginate droplets were crosslinked with Ca^{2+} to form Ca-alginate microparticles. In the current study, the throughput of the device was evaluated by the numbers of the cell-encapsulated microparticles produced at one run. When the flow rates of the dispersed phase and the continuous phase were respectively set at 1.5 μL min^{-1} and 3 μL min^{-1}, we can produce hundreds of cell-encapsulated microparticles at one run and more than 65% of the formed cell aggregates in the microparticles had the same shapes (Fig. S6, ESI†). To compare with the conventional approaches,[34-36] the use of the microfluidic droplet method greatly improves the throughput of the cell aggregates. Due to the limitation of the device structures, the conventional approaches could only produce dozens of cell aggregates at one run. For examples, in Dean's work, limited by the number of the micromolds, they could produce no more than one hundred of cell aggregates at one run.[34] By using the micromolding methods, Tekin et al. could also produce dozens of cell aggregates at one run.[35,36] In addition, comparing with the on-chip system for the formation of alginate hydrogel microparticles,[51] the current approach used an off-chip Ca^{2+} bath for the gelation of Na-alginate droplets, which avoided the blocking issue frequently encountered by the on-chip gelation.
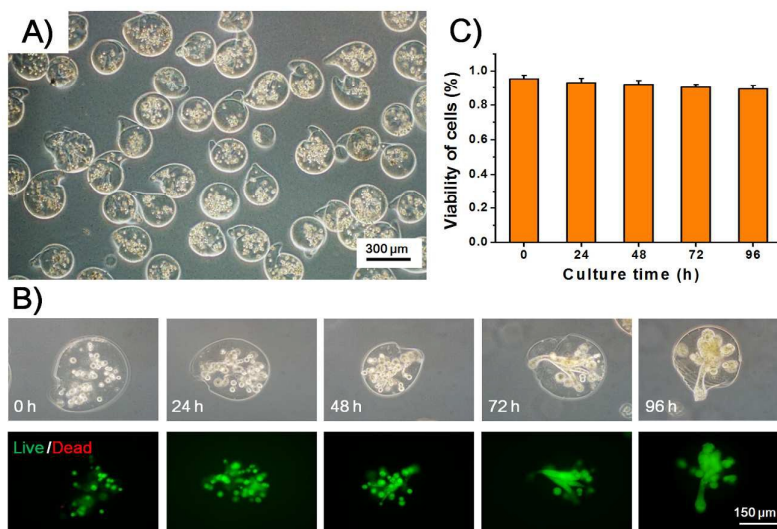
Fig. 2 A) A typical image of HeLa cells encapsulated in 2% alginate and 5% $CaCl_2$ microparticles. B) Time-sequence images of viability and proliferation of HeLa cells encapsulated in 2% alginate and 5% $CaCl_2$ microparticles. C) Viability analysis of HeLa cells in the microparticles during different culture times.

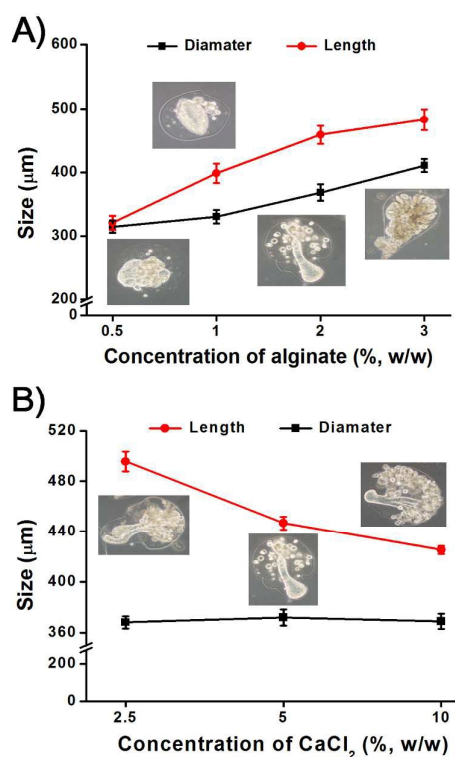### Ca-alginate microparticle generation and cell aggregate formation

It is well known that exposure to oil is harmful for mammal cells.[52] In the current system, not only the process of alginate droplet formation but also the off-chip gelation gives cells the chance to contact with mineral oil. Thus, to test whether the system was suitable for cell culture, the Ca-alginate microparticles encapsulating HeLa cells were first prepared under conventional conditions and cultured for 96 h.[26,38] Generally, 2% w/w sodium alginate in cell-contained DMEM and mineral oil containing 2% w/w Span 80 were respectively introduced into the microdevice through the curved and oil channels. The oil and alginate solution met at the cross junction and spontaneously generated droplets due to their different interfacial properties.[48] After traveling downstream and dripping into the reservoir, the Na-alginate droplets underwent a crosslinking reaction in the $CaCl_2$ bath and finally formed the Ca-alginate microparticles. The formed microparticles were immediately transferred into fresh DMEM, in which tail-shaped alginate hydrogel microparticles containing a few tens of HeLa cells were generated (Fig. 2A). The reason for the formation of the tail-shaped microparticles may be due to localized gelation occurred during the crosslinking reaction. When the Na-alginate droplets reached the interface between the oil and $CaCl_2$ solution in the reservoir pool, sodium alginate droplets

reacted with Ca^{2+}, initiating gelation. Gelation and movement to the aqueous phase of the Na-alginate droplets occurred at the same time.[53] The lower part of the droplet in contact with the aqueous phase become gel, however, the other part of the droplet still placed in the oil phase and kept the spherical shape, which disequilibrated the surface tension of the droplets. As a result, the imbalance in surface tension and additional force due to the partial gelation make a tail-shaped microparticle.[54]

To test the capability of the current approach for cell aggregate formation, the growth of cells encapsulated in the microparticles was monitored for 96 h under standard culture condition. Cell images (Fig. 2B) at 0, 24, 48, 72 and 96 h exhibited their proliferation. Initially, HeLa cells were randomly distributed throughout the Ca-alginate microparticles. As time passed, the sparse cells in the microparticles proliferated along the tail and became dense and compact. After 96-h culture, cells merged to form a branch-like aggregate in the alginate microparticle. Live/dead cell staining assay[44] showed that during the whole culture period the viability of cells was more than 90% (Fig. 2C), indicating that the exposure to mineral oil was not harmful to the cells. This phenomenon could be attributed to the use of the biocompatible M8410 mineral oil[55] and the rapid transfer of the formed microparticles into DMEM. The results indicated that HeLa cells in non-spherical Ca-alginate microparticles would form non-spherical aggregates, which means that the morphological and dimensional characteristics of alginate microparticles may have influences on the shape and size of the cell aggregates. This conclusion is in accord with the perspective proposed in the previous studies,[25,26] in which the morphological and dimensional characteristics of hydrogel microparticles played a crucial role in the formation of cell aggregates.

Effects of alginate concentration

One of the most vital influencing factors to the morphology of Ca-alginate microparticles is the concentration of alginate.[53] Considering the shape and size of Ca-alginate microparticles have influences on cell aggregates, the effects of alginate concentration on the shape and size of microparticles and cell aggregates were investigated in the current study. Various Ca-alginate microparticles encapsulated HeLa cells (Fig. S1, ESI†) were prepared with different concentrations of alginate (0.5%, 1%, 2% and 3%). 5% w/w $CaCl_2$ was used as the crosslinking reagent in this study. The formed Ca-alginate microparticles had uniform shape and size. The diameter and length (Fig. 3A, Fig. S4 and Table S1, ESI†) of the Ca-alginate microparticles were 314 ± 15 μm and 320 ± 19 μm for 0.5% alginate, 330 ± 17 μm and 398 ± 25 μm for 1% alginate, 368 ± 16 μm and 458 ± 24 μm for 2% alginate, and 410 ± 19 μm and 482 ± 19 μm for 3% alginate. In each group (Fig. S3, ESI†), there were unconspicuous differences (no more than 30 μm) in both diameter and length of more than 80% Ca-alginate microparticles (n = 100). The ANOVA test (Fig. S4, ESI†) showed that there were statistically significant differences in both length and diameter as a function of alginate concentration (p<0.001). In addition, the results (Fig. 3A) revealed that both the length and diameter of the microparticles increased with the

Fig. 3 Effect of alginate and $CaCl_2$ concentration on the shape and size of the microparticles and HeLa cell aggregates. A) Effect of alginate concentration on the diameter and length of Ca-alginate microparticles. Inserts: typical micrographs of corresponding HeLa cell aggregates after 96-h culture. 5% (w/w) $CaCl_2$ was used in this study. B) Effect of $CaCl_2$ concentration on the diameter and length of Ca-alginate microparticles. Inserts: typical micrographs of corresponding HeLa cell aggregates after 96-h culture. 2% alginate was used in this study.

increase of alginate concentration. This phenomenon could be attributed to the increase of the viscosity of alginate solutions, caused by the increase of alginate concentration. When the water in oil droplets formed at the cross-junction, the viscosity of the dispersed phase had a vital influence on the size of the droplets that the more viscous the alginate solution was the bigger the formed droplets were.[43] The big alginate droplets experienced long localized gelation process (discussed in the previous section), resulting in the increase of tail length of the formed Ca-alginate microparticles. In addition, the increase in diameter of droplets made a corresponding increase in diameter of microparticles. Thus, a positive correlation was obtained between the concentration of alginate solution and the diameter and length of Ca-alginate microparticles.

The influnce of alginate concentration on the shape and size of cell aggregates was also studied. As shown in Fig. 3A, HeLa cell aggregates with spherical, spindle-like (the spindle shapes was classified in one trunk without branches) and branch-like shapes (the branch shape was classified in one trunk with some branches) were obtained in their corresponding microparticles after 96-h culture. The diameters of the spherical and spindle-like cell aggregates were 174 ± 11 μm and 190 ± 15 μm, respectively. The length of the branch-like cell aggregates was 344 ± 4 μm. It should be noted that cell aggregates with irregular shapes were found in 3% w/w Ca-alginate microparticles. This phenomenon may be attributed to the fact that the high concentration of alginate made the inner structure of microparticles became irregular, which lead to the formation of irregular cell aggregates. To further demonstrate the versatility of this cell clustering technology, the other two types of cell lines (HepG2 and HUVECs) were also examined and the same results were obtained (Fig. S5, ESI†). All the results revealed that as the alginate concentration increased from 0.5% to 2%, the shape of the cellular aggregate transformed from
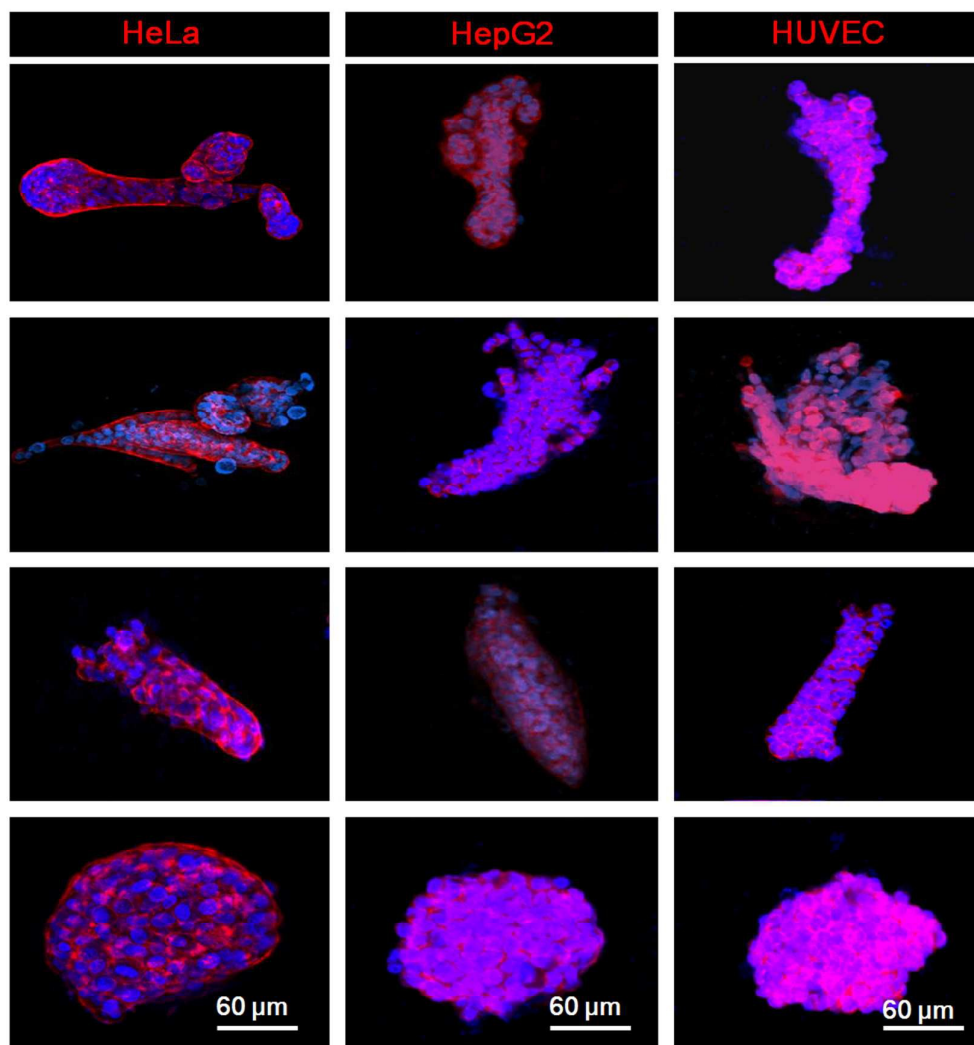

Fig. 4 Typical fluorescence images of HeLa, HepG2 and HUVEC aggregates formed in different Ca-alginate microparticles. From top to bottom: the concentration of alginate and CaCl₂ used for the formation of the microparticles were 2% and 5%, 2% and 2.5%, 1% and 5%, and 0.5% and 5%, respectively. Cell aggregates were stained with rhodamine phalloidin (red) and Hoechst 33258 (blue).

sphere to spindle to branching. The formed cell aggregates seemed been drawn-out accompanying by the increase of alginate concentration, which was in accordance with the effect of alginate concentration (Fig. 3A) on the shape and size of microparticles. In addtion, these results implied that the shape and size of cell aggregates were decided by the inner structure of the Ca-alginate microparticles. To prove the shapes of various cell aggregates are reproducible, the percentage of cell aggregates in a population of microbeads was summed up (Fig. S6, ESI†). In the spheroid, spindle-like and branch-like groups, the percentages were 67.35% ± 3.11%, 65.36% ± 2.92% and 69.32% ± 3.53%, respectively. In each group, the percentages of cell aggregates with the same shapes are all more than 65%, demonstrated that each shape is reliably produced using its corresponding alginate and $CaCl_2$ concentrations.

Effects of $CaCl_2$ concentration

Sodium alginate crosslink with divalent cations such as Ca^{2+} to gelation,[37] in which the concentration of Ca^{2+} has vital influence on the speed of gelation.[53] In the current study, the gelation of alginate droplet experienced a localized gelation process, resulted in the formation of tail-shaped microparticles. Thus, to find out if the concentration of $CaCl_2$ affects the shape and size of the formed Ca-alginate microparticles and cell

aggregates, various Ca-alginate microparticles encapsulating HeLa cells (Fig. S7, ESI†) were prepared with different $CaCl_2$ concentrations (2.5%, 5% and 10%; 2% w/w alginate was used in the study). The formed Ca-alginate microparticles possessed tail-shape and uniform in size. The diameter and length of Ca-alginate microparticles (Fig. 3B, Fig S9 and Tabel S2, ESI†) are 366 ± 13 μm and 495 ± 18 μm for 2.5% $CaCl_2$, 368 ± 14 μm and 446 ± 19 μm for 5% $CaCl_2$, and 367 ± 15 μm and 425 ± 17 μm for 10% $CaCl_2$. In each group (Fig. S8, ESI†), there were unconspicuous differences (no more than 30 μm) in both diameter and length of more than 80% Ca-alginate microparticles (n =100). The ANOVA test (Fig. S9, ESI†) demonstrated that there was statistically significant difference in length but no significant difference in diameter as a function of $CaCl_2$ concentration (p<0.001). The length of the Ca-alginate microparticles was inversely proportional to the $CaCl_2$ concentration, indicating that the concentration of $CaCl_2$ has a vital influnce on the tail length of the microparticles. A higher concentration of $CaCl_2$ during gelation made the tails of the formed microparticles becoming shorter. This phenomenon could be attributed to the fact that localized gelation occurred during the crosslinking reaction, which resulted in the formation of tail-shaped Ca-alginate microparticles. The longer the gelation time the longer the length of tail is. Under the fixed
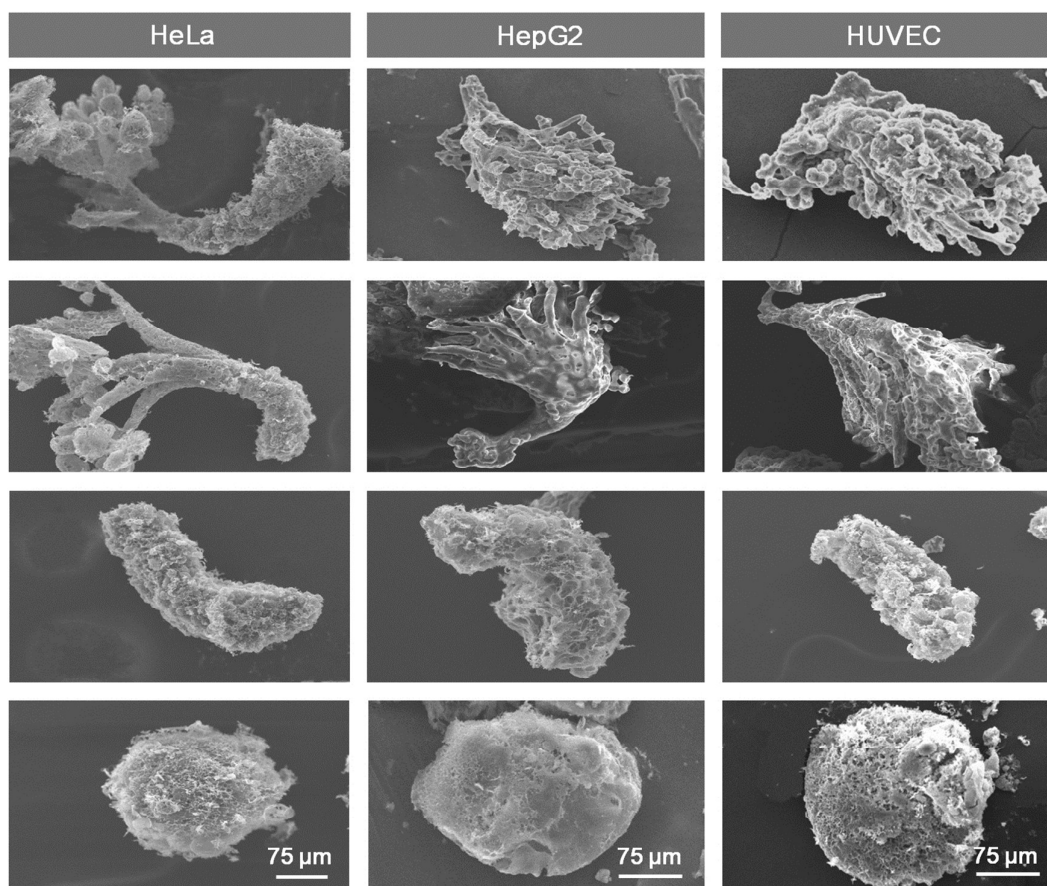

Fig. 5 SEM images of HeLa, HepG2 and HUVEC aggregates formed in different Ca-alginate microparticles. From top to bottom: the concentration of alginate and $CaCl_2$ used for the formation of the microparticles were 2% and 5%, 2% and 2.5%, 1% and 5%, and 0.5% and 5%, respectively.

Paper

Analytical Methods

concentration of alginate, the concentration of Ca^{2+} was proportional of the gelation time.[56] As a result, the dense Ca^{2+} accelerated the gelation process and led to a short tail. However, the diameters of the microparticles seem not be affected by the concentration of $CaCl_2$ since no significant difference in the diameters of the Ca-alginate microparticles formed under different $CaCl_2$ concentrations (Fig. 3B). The diameter of the microparticles was mainly determined by the size of the Na-alginate droplets formed at the cross junction of the microdevice.

The influnce of $CaCl_2$ concentration on the shape and size of cell aggregates was also studied. HeLa cells were encapsulated and cultured in various Ca-alginate microparticles formed under different $CaCl_2$ concentrations (2.5%, 5% and 10%). After 96-h culture, branch-like cell aggregates were obtained (Fig. 3B). The length of the branch-like cell aggregates was 416 ± 15 μm for 2.5% $CaCl_2$, 344 ± 22 μm for 5% $CaCl_2$ and 312 ± 19 μm for 10% $CaCl_2$, which was inversely proportional to $CaCl_2$ concentration. The same phenomenon was also observed in the tests of HepG2 and HUVECs (Fig. S10, ESI†), which could be attributed to the decrease of Ca-alginate microparticle length due to the increase of $CaCl_2$ concentration, similar with the effect of $CaCl_2$ concentration on the size of alginate particles (Fig. 3B).
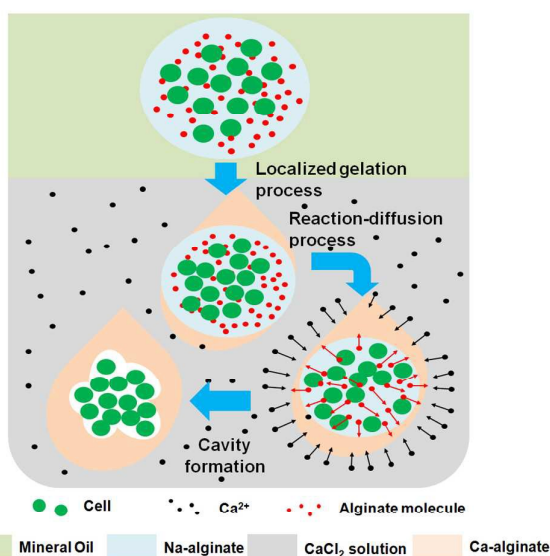
Cytoskeleton and morphological analysis of the cell aggregates

In vivo, cell-cell interaction refers to the direct interactions between cell surfaces that play a crucial role in the development and function of multicellular organisms.[57] Thus, creating 3D cell-to-cell contact is a crucial element for building blocks in

Fig. 6 The schematic diagram of cell aggregate formation with specific shapes. Firstly, the alginate droplets encapsulated cells experienced the localized gelation process at the interface between mineral oil and $CaCl_2$ solution, which induced the formation of the external morphology of the Ca-alginate microparticles. Then, the reaction-diffusion process leaded to the formation of cavities inside the Ca-alginate microparticles. Because of the spatial constraints, the cells would proliferate and fuse to an aggregate with a specific shape, same with that of the cavity. The red and black arrows respectively represent the movements of alginate molecules and Ca^{2+}.

tissue engineering. To visually observe the cell-cell connection in the cell aggregates formed in the Ca-alginate microparticles, cytoskeleton of cells in the cell aggregates was stained with TRITC-phalloidin, a chemical that can bind to F-actin of cells.[58] The nuclei of cells were stained with H33258 fluorochrome. The results (Fig. 4 and Figs. S11-S13, ESI†) showed that in the spherical and spindle-like aggregates the cells well attached each other without empty spaces. However, in the branch-like cell aggregates there were spaces between cells. These phenomena could be attributed to the different alginate concentrations which had influnces on the inner structure of Ca-alginate microparticles.[53] When Na-alginate droplets were introduced into $CaCl_2$ solution, the alginate reacted with calcium to form alginate-calcium. In fact, the gelation of alginate is a reaction-diffusion process, in which two chemicals (calcium and alginate) diffuse towards each other over a constant constituting boundary to form a stable structure: the Ca-alginate gel network.[53] In the low alginate concentration groups (spheroidic and spindle-like), a small amount of alginate allows for a rapid penetration of calcium ions. Inversely, in the high alginate concentration group (branch-like), a mass of alginate slows the penetration of calcium ions. Thus, the reaction of alginate with calcium was not sufficient in the high concentration group. As a result, more empty spaces were generated in the inner structure of the Ca-alginate microparticles in the high concentration group than those in the low concentration groups. Fortunately, these empty spaces did not disturb the formation of branch-like cell aggregates. After dissolving the Ca-alginate microparticles in 55 mM sodium citrate, intact branch-like cell aggregates were successfully obtained (Fig. 5 and Fig. S15, ESI†). To further demonstrate that the formed cell aggregates were densely packed and interconnected, SEM observation was also performed. As showed in Fig. 5, the surfaces of the cell aggregates were compact, suggesting that the cells were densely packed and interconnected. Further more, the formed cell aggregates were intact, which means neither the empty spaces formed in the branch-like group nor the retrieval method had vital influences on the structure of cell aggregates.

Mechanism of the formation of shape-controlled cell aggregates

According to the results obtained above, the mechanism of the formation of shape-controlled cell aggregates was speculated. Generally, the morphology of cell aggregates was decided by the inner structure of Ca-particles. During the alginate gelation process, various events take place simultaneously or gradually that caused the formation of the inner structure of Ca-alginate microparticles (Fig. 6). In more detail, when the Na-alginate droplets reached the interface between the oil and $CaCl_2$ solution in the reservoir pool, sodium alginate droplets reacted with Ca^{2+}, initiating gelation. Gelation and movement to the aqueous phase of Na-alginate droplets occurred at the same time.[53] The lower part of the droplet contacted with the aqueous phase become gel, however, the other part of the droplet still placed in the oil phase and kept the spherical shape, which disequilibrated the surface tension of the droplets. As a result, the imbalance in surface tension and additional force due to the

partial gelation make a tail-shaped microparticle. This localized gelation process that was affected by the concentrations of alginate and $CaCl_2$ (discussed in the sections of Effects of alginate and $CaCl_2$ concentrations) determined the entire morphology of the Ca-alginate microparticles. On the other hand, at the begining of the gelation, the formation of a superficial crust acting as a spherical belt progressively tightens the gel microparticle.[59] This kind of structure is a continuous increasing obstacle to the diffusion of calcium within the forming gel microparticle. Additionally, the reaction-diffusion process slowed down the speed of reaction.[53] The process and tightening of the superficial crust provoke the syneresis, which caused the reduction of the gel microparticles. Meanwhile, the unreacted alginate molecules move progressively from the bead center to the moving boundary of the reaction front, attracted by the accumulation of calcium ions at this interface.[53] All the events produce a cascade of reaction-diffusion processes provoking the formation of the inner cavities of Ca-alginate microparticles, which provides the space for cell proliferation. In addition, the concentration of alginate and $CaCl_2$ affects the entire morphology of the Ca-alginate microparticles and the speed of these reaction-diffusion processes, resulted in the formation of inner cavities with different shapes: at the lowest concentration of alginate, the shapes of Ca-alginate microparticles were spheroid. Thus, the unreacted alginate molecules inside the microparticles moved around the spherical surface layer and resulted in the formation of spherical cavities; at the medium concentration of alginate, the partial gelation process made a tail-shaped microparticle and resulted in the formation of spindle-like cavities; at the higher concentration of alginate, the increased diameter and tail length (discussed in the

section of Effects of alginate concentration) of the microparticles and the higher number of alginate molecule resulted in the formation of branch-like cavities. The concentration of $CaCl_2$ affected the speed of gelation that resulted in the changes of the length of inner cavities: at lower Ca^{2+} concentration, the localized gelation process and the reaction-diffusion process lasted a longer time and elongated the inner cavities; at higher Ca^{2+} concentration, the dense Ca^{2+} accelerated the gelation process and led to a shorter inner cavity. Consequently, under the combined effect of partial gelation and reaction-diffusion process, cells encapsulated in the Ca-alginate microparticles that were prepared under different concentrations of alginate and $CaCl_2$ self-assembled into the internal structure-corresponded cell aggregates due to the growing space constraint.

To prove the hypothesis, the inner structures of the Ca-alginate microparticles were directly observed using the semi-thin section of epoxy resin method.[46] Briefly, the Ca-alginate microparticles were first embedded into epoxy resin and cut off into 2-μm slices with LEICA Rm 2265 microtome. To visualize the inner structures of the Ca-alginate microparticles, the slices were then stained with positively charged methylene blue, during which only alginate could be stained blue.[47] The blank areas were the cavities /empty spaces in the microparticles. The results (Fig. 7) showed that four types of cavities, spindle-like (Fig. 7A), spheroid-like (Fig. 7B), branch-like (Figs. 7C-E) and irrgular (Fig. 7F) shapes, were formed in the microparticles. Moreover, each type of cavity corresponded its own preparation conditions and one shape of cell aggregate. The results demonstrated that the spatial constraints result in the formation of various shapes of cell aggregates. In other words, the shape
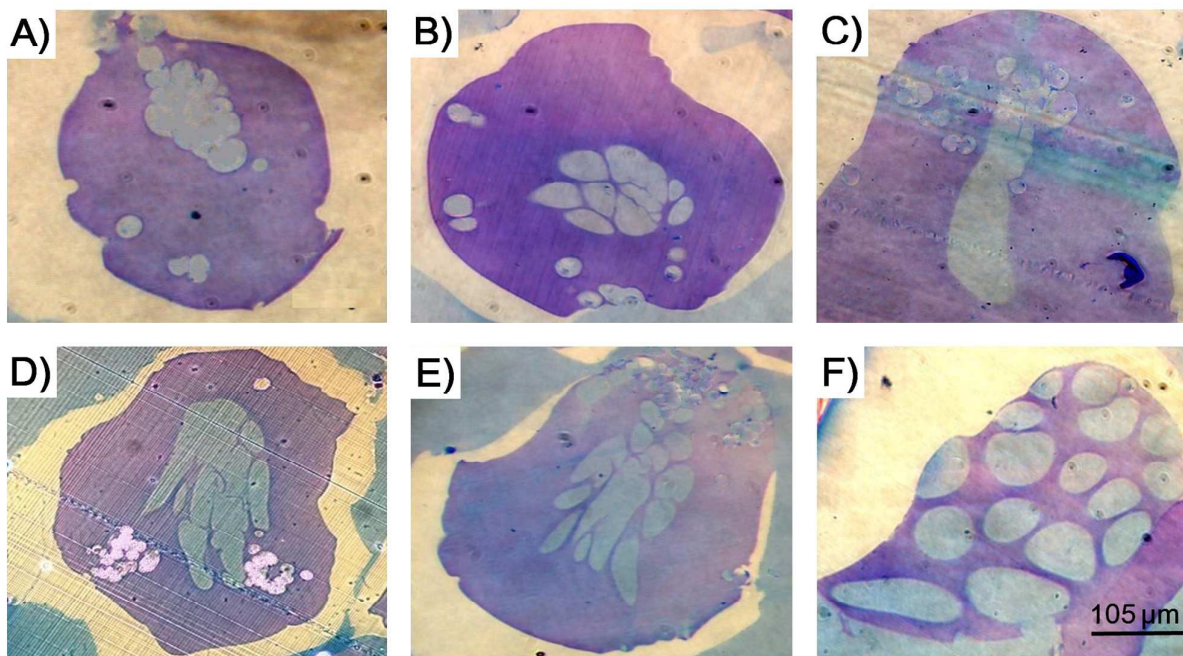

Fig. 7 Typical micrographs of the section of Ca-alginate microparticles colored with methylene blue. The blank areas represent the cavities /empty spaces in the microparticles. The concentrations of alginate and $CaCl_2$ used for the formation of the microparticles were respectively 1% and 5% (A), 0.5% and 5% (B), 2% and 2.5% (C), 2% and 5% (D), 2% and 10% (E), and 3% and 5% (F).

Paper

Analytical Methods

and size of the formed cell aggregates were decided by the inner structures of Ca-alginate microparticles, which can be controlled by regulating their preparation conditions.

Retrieval and re-culture of the cell aggregates

Retrieval of tissue building blocks is a desirable property of micro-fabricated culture templates.[36] To demonstrate the current method possesses this property, Ca-alginate microparticles containing cell aggregates were introduced into 55 mM sodium citrate and the time-sequenced images of the cell aggregate retrieval from Ca-alginate microparticles were recorded (Fig. S14, ESI†), exhibiting that the boundary of the Ca-alginate microparticles (red arrow) became blurry with time passed and totally disappeared after 10 min. This phenomenon was caused due to the reason that Ca-alginate microparticles were liquefied by chelation.[60] Citrate chelates Ca^{2+} more easily than alginate, so that when the microparticles were introduced into sodium citrate, Ca^{2+} in Ca-alginate was replaced by Na^+, resulting in liquefying. Cell viability assays by using the AO/PI double-staining protocol[44] showed that the viability of the cells on the surfaces of the retrieved cell aggregates were all more than 95% (Fig. S15, ESI†). To further investigate the viability and integrity of cells inside the cell aggregates, the retrieved cell aggregates were re-cultured using the conventional cell culture method and the time dependent images were recorded (Figs. S16-S18, ESI†), indicating that the cells have good morphology and proliferation ability. Live/dead cell staining assay showed that all the cells have high viability (>95%), similar to the cells on the surfaces of the cell aggregates. All the results implied that the current approach for the formation of cell aggregates does not compromise cell viability and integrity.

Conclusions

In summary, we successfully developed a microfluidic droplet-based approach that enabled the production of cell aggregates with different shapes in Ca-alginate microparticles. Combined with the conventional protocol used for the formation of cell-encapsulated Ca-alginate microparticles, we successfully obtained cell aggregates with different shapes. In addition, the results also demonstrate that the shape of the cell aggregates can be tailored by changing the concentrations of alginate and $CaCl_2$. Cytoskeletal analysis and SEM observation showed that the formed cell aggregates were densely packed and interconnected. Reculture process demonstrated that the cell aggregates maintained high viability (>95%) after being harvested from the Ca-alginate microparticles by chelation using sodium citrate. Study on the formation mechanism revealed that the shapes and sizes of the cell aggregates were mainly decided by the inner structures of Ca-alginate microparticles, which can be controlled by regulating their preparation conditions. Considering the simplicity, controllability, applicability and practicality of this approach, we envision that the microfluidic approach might be an efficient tool for the production of cell aggregates with different shapes, and could be used for the application that requires

modular tissue formation and experimentation, such as tissue engineering, imaging and drug discovery.

Acknowledgements

Notes and references

1 P. Zorlutuna, N. Annabi, G. Camci-Unal, M. Nikkhah, J. M. Cha, J.W. Nichol, A. Manbachi, H. Bae, S. Chen, A. Khademhosseini, *Adv Mater*, 2012, **24**, 1782.
2 R. Langer, J. P. Vacanti, *Science*, 1993, **260**, 920.
3 B. Guillotin, F. Guillemot, *Trends Biotechnol*, 2011, **29**, 183.
4 S. Korossis, F. Bolland, J. Southgate, E. Ingham, J. Fisher, *Biomaterials*, 2009, **30**, 266.
5 I. Wimpenny, N. Ashammakhi, Y. Yang, *J Tissue Eng Regen Med*, 2012, **6**, 536.
6 F. Groeber, M. Holeiter, M. Hampel, S. Hinderer, *Clin Plast Surg*, 2012, **39**, 33.
7 T. Lu, Y. Li, T. Chen, *Int J Nanomedicine*, 2013, **8**, 337.
8 J. S. Liu, Z. J. Gartner, *Trends Cell Biol*, 2012, **22**, 683.
9 D. L. Elbert, *Curr Opin Biotechnol*, 2011, **22**, 674.
10 J. W. Nichol, A. Khademhosseini, *Soft Matter*, 2009, **5**, 1312.
11 A. Leferink, D. Schipper, E. Arts, E. Vrij, N. Rivron, M. Karperien, K. Mittmann, C. van Blitterswijk, L. Moroni, R. Truckenmüller, *Adv Mater*, 2014, **26**, 2592.
12 E. Fennema, N. Rivron, J. Rouwkema, C. van Blitterswijk, J. de Boer, *Trends Biotechnol*, 2013, **31**, 108.
13 S. L. Nyberg, B. Amot, U. A. Arquikar, R. P. Remmel, P. Rinaldo, *Liver Transplant*, 2005, **11**, 901.
14 M. Ingram, G. B. Techy, R. Saroufeem, O. Yazan, K. S. Narayan, T. J. Goodwin, G. F. Spaulding, *In Vitro Cell Dev Biol: Anim*, 1997, **33**, 459.
15 J. B. Kim, R. Stein, M. J. O'Hare, *Breast Cancer Res Treat*, 2004, **85**, 281.
16 R. L. Carpenedo, C. Y. Sargent, T. C. McDevitt, *Stem Cells*, 2007, **25**, 2224.
17 P. Manley, P. I. Lelkes, *J Biotechnol*, 2006, **125**, 416.
18 S. Sakai, S. Ito, K. Kawakami, *Acta Biomater*, 2010, **6**, 3132.
19 W. Zhang, S. Zhao, W. Rao, J. Snyder, J. K. Choi, J. Wang, I. A. Khan, N. B. Saleh, P. J. Mohler, J. Yu, T. J. Hund, C. Tang, X. He, *J Mater Chem B Mater Biol Med*, 2013, **2013**, 1002.
20 J. L. Wilson, T. C. McDevitt, *Biotechnol Bioeng*, 2013, **110**, 667.
21 M. Y. Lee, R. A. Kumar, S. M. Sukumaran, M. G. Hogg, D. S. Clark, J. S. Dordick, *Proc Natl Acad Sci U.S.A.*, 2008, **105**, 59.
22 K. H. Lee, Y. No da, S. H. Kim, J. H. Ryoo, S. F. Wong, S. H. Lee, *Lab Chip*, 2011, **11**, 1168.

23 M. C. Chen, M. Gupta, K.C. Cheung, *Biomed Microdevices*, 2010, **12**, 647.

24 S. Yoon, J. A. Kim, S. H. Lee, M. Kim, T. H. Park, *Lab Chip*, 2013, **13**, 1522.

25 K. Alessandri, B. R. Sarangi, V. V. Gurchenkov, B. Sinha, T. R. Kießling, L. Fetler, F. Rico, S. Scheuring, C. Lamaze, A. Simon, S. Geraldo, D. Vignjevic, H. Doméjean, L. Rolland, A. Funfak, J. Bibette, N. Bremond, P. Nassoy, *Proc Natl Acad Sci U.S.A.*, 2013, **110**, 14843.

26 Y. Wang, J. Wang, *Analyst*, 2014, **139**, 2449.

27 H. Suga, T. Kadoshima, M. Minaguchi, M. Ohgushi, M. Soen, T. Nakano, N. Takata, T. Wataya, K. Muguruma, H. Miyoshi, S. Yonemura, Y. Oiso, Y. Sasai, *Nature*, 2011, **480**, 57.

28 N. Lumelsky, O. Blondel, P. Laeng, I. Velasco, R. Ravin, R. McKay, *Science*, 2001, **292**, 1389.

29 I. Kehat, D. Kenyagin-Karsenti, M. Snir, H. Segev, M. Amit, A. Gepstein, E. Livne, O. Binah, J. Itskovitz-Eldor, L. Gepstein, *J Clin Invest*, 2001, **108**, 407.

30 J. Yeh, Y. Ling, J. M. Karp, J. Gantze, A. Chandawarkard, G. Eng, J. Blumling, R. Langer, A. Khademhosseini, *Biomaterials*, 2006, **27**, 5391.

31 N. C. Rivron, E. J. Vrij, J. Rouwkema, S. Le Gac, A. van den Berg, R. K. Truckenmüller, C. A. van Blitterswijk, *Proc Natl Acad Sci U.S.A.*, 2012, **109**, 6886.

32 Y. Zhao, R. Yao, L. Ouyang, H. Ding, T. Zhang, K. Zhang, S. Cheng, W. Sun, *Biofabrication*, 2014, **6**, 035001.

33 W. H. Tan, S. Takeuchi, *Adv Mater*, 2007, **19**, 2696.

34 D. M. Dean, A. P. Napolitano, J. Youssef, J. R. Morgan, *FASEB J.*, 2007, **21**, 4005.

35 H. Tekin, T. Tsinman, J. G. Sanchez, B. J. Jones, G. Camci-Unal, J. W. Nichol, R. Langer, A. Khademhosseini, *J Am Chem Soc*, 2011, **133**, 12944.

36 H. Tekin, G. Ozaydin-Ince, T. Tsinman, K. K. Gleason, R. Langer, A. Khademhosseini, M. C. Demirel, *Langmuir*, 2011, **27**, 5671.

37 K. Liu, H. J. Ding, J. Liu, Y. Chen, X. Z. Zhao, *Langmuir*, 2006, **22**, 9453.

38 L. Yu, M. C. Chen, K. C. Cheung, *Lab Chip*, 2010, **10**, 2424.

39 K. Y. Lee, D. J. Mooney, *Prog Polym Sci*, 2012, **37**, 106.

40 L. Wang, W. Liu, Y. Wang, J. C. Wang, Q. Tu, R. Liu, J. Wang, *Lab Chip*, 2013, **13**, 695.

41 X. Huang, L. Li, Q. Tu, J. Wang, W. Liu, X. Wang, L. Ren, J. Wang, *Microfluid Nanofluid*, 2011, **10**, 1333.

42 J. C. Wang, W. Liu, Q. Tu, C. Ma, L. Zhao, Y. Wang, J. Ouyang, L. Pang, J. Wang, *Analyst*, 2015, **140**, 827.

43 C. N. Baroud, F. Gallaire, R. Dangla, *Lab Chip*, 2010, **10**, 2032.

44 W. Liu, L. Li, J. C. Wang, Q. Tu, L. Ren, Y. Wang, J. Wang, *Lab Chip*, 2012, **12**, 1702.

45 L. Ren, W. Liu, Y. Wang, J. C. Wang, Q. Tu, J. Xu, R. Liu, S. F. Shen, J. Wang, *Anal Chem*, 2013, **85**, 235.

46 D. Mitrecić, V. F. Cunko, S. Gajović, *J Microsc*, 2008, **232**, 504.

47 M. Rafatullah, O. Sulaiman, R. Hashim, A. Ahmad, *J Hazard Mater*, 2010, **177**, 70.

48 E. W. Kemna, R. M. Schoeman, F. Wolbers, I. Vermes, D. A. Weitz, A. van den Berg, *Lab Chip*, 2012, **16**, 2881.

49 R. You, H. Haj-Hariri, A. Borhan, *Phys Fluids*, 2009, **21**, 013102.

50 Y. Hu, Q. Wang, J. Wang, J. Zhu, H. Wang, Y. Yang, *Biomicrofluidics*, 2012, **6**, 26502.

51 C. H. Choi, J. H. Jung, Y. Rhee, D. P. Kim, S. E. Shim, C. S. Lee, *Biomed Microdevices*, 2007, **9**, 855.

52 D. Fabian, M. Sabol, K. Domaracká, D. Bujnáková, *Toxicol In Vitro*, 2006, **20**, 1435.

53 C. Bienaimé, J. N. Barbotin, J. E. Nava-Saucedo, *J Biomed Mater Res A*, 2003, **67**, 376.

54 Y. S. Lin, C. H. Yang, Y. Y. Hsu, C. L. Hsieh, *Electrophoresis*, 2013, **34**, 425.

55 T. Watanabe, A. Thayil, A. Jesacher, K. Grieve, D. Debarre, T. Wilson, M. Booth, S. Srinivas, *BMC Cell Biol.*, 2010, **11**, 38.

56 T. D. Dang, S. W. Joo, *Colloids Surf B Biointerfaces*, 2013, **102**, 766–71.

57 T. Lu, Y. Li, T. Chen, *Int J Nanomedicine*, 2013, **8**, 337.

58 X. Wang, F. Wei, A. Liu, L. Wang, J. C. Wang, L. Ren, W. Liu, Q. Tu, L. Li, J. Wang, *Biomaterials*, 2012, **33**, 3719.

59 A. Blandino, M. Macias, D. Cantero, *J Biosci Bioeng* 1999, **88**, 686.

60 S. Sakai, H. Inagaki, Y. Liu, T. Matsuyama, T. Kihara, J. Miyake, K. Kawakami, M. Taya, *Biotechnol Bioeng*, 2012, **109**, 2911.

Graphic abstract
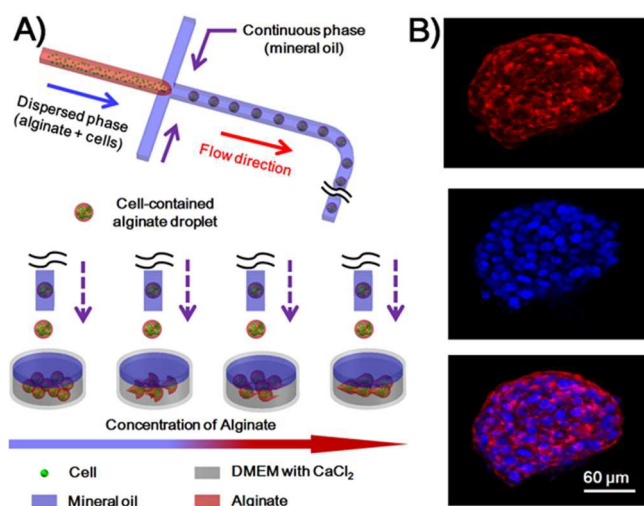
We present a microfluidic droplet-based approach that can easily produce different shapes of cell aggregates in Ca-alginate microparticles by changing alginate and $CaCl_2$ concentrations.